Available online at www.sciencedirect.com
SCIENCE DIRECT®
Journal of Computational Physics 208 (2005) 266–288
JOURNAL OF COMPUTATIONAL PHYSICS
www.elsevier.com/locate/jcp

Convergence characteristics of preconditioned Euler equations

Sang-Hyeon Lee *

Department of Aerospace Engineering, University of Ulsan, Moogu-Dong, Nam-Gu, Ulsan 680-749, Republic of Korea

Received 30 August 2004; received in revised form 10 February 2005; accepted 14 February 2005
Available online 13 April 2005

Abstract

The convergence characteristics of the preconditioned Euler equations were studied. A perturbation analysis was conducted to search for the relationships between the convergence characteristics and the flow Mach numbers. Also, the influence of cancellation errors on the convergence characteristics was investigated. The governing equations were the preconditioned two-dimensional Euler equations. Flows in a two-dimensional channel with a 10% circular bump in the middle of the channel were calculated at different speeds. Roe's FDS scheme was used for spatial discretization and the LU-SGS (Lower Upper Symmetric Gauss Seidel) scheme was used for time integration. It was shown that the convergence characteristics of continuity and momentum equations were maintained regardless of the Mach numbers, but the convergence characteristics of energy equation were strongly dependant on the Mach numbers and worsened as the Mach number decreased. The convergence characteristics were well explained by the perturbation analysis. The convergence characteristics were strongly dependant on the characteristics of the preconditioning matrix. Cancellation errors caused a serious convergence problem especially in the calculation of the energy equation at very low Mach numbers. The relative treatments and a higher precision of floating-point variables alleviated cancellation problems to some extent. However, the convergence rate was not affected by the relative treatments or by the precision of floating-point variables.

1. Introduction

There is a great need for compressible algorithms to solve thermo-fluid-dynamic problems in low speed flows. Incompressible algorithms are insufficient for low speed flows in which compressible effects are dominant. Typical examples of compressible low speed flows can be found in natural convection flows in gas or

* Tel.: +82 52 259 2825; fax: +82 52 259 1681.
E-mail address: lsh@mail.ulsan.ac.kr.

0021-9991/$ - see front matter © 2005 Elsevier Inc. All rights reserved.
doi:10.1016/j.jcp.2005.02.014

liquid phase, subsonic combustion in heat engines or burners, heat transfer in heat exchangers, and others. Also, many flows involve a wide range of Mach number variation. Some examples include rocket motor flows in which the Mach number is zero at the closed end and supersonic at the divergent nozzle exit, high-speed flows with large embedded recirculation zones, multi-phase flows in which the Mach number changes drastically through the phase boundaries, and flow over a wing at high angle of attack. However, it is very difficult or impossible to solve low speed flows with a conventional compressible algorithm because of slow convergence. The difficulty in solving the compressible equations for low Mach numbers is associated with the large disparity between the acoustic wave speed and the waves propagating at the fluid speed, which is called eigenvalue stiffness. Preconditioning methods have been suggested to overcome this stiffness problem. The preconditioning method pre-multiplies the time derivative by a suitable matrix that scales the eigenvalues of a system of equations to the same order of magnitude, which makes it possible to provide a solution valid for all Mach numbers.

There have been many research activities focused toward developing effective preconditioning algorithms. The algorithm suggested by Viviand [1] was one of the first and the most complete, stating a generalized preconditioning procedure for a class of hyperbolic systems of equations and specific rules for ensuring that the preconditioned equations remain well posed. Peyret and Viviand [2] presented additional detailed considerations for preconditioning algorithms. After these works, a number of studies reported significant improvements in preconditioning methods [3–6]. Choi and Merkle [7] suggested a preconditioning matrix that introduced well-conditioned eigenvalues and pressure gradient terms. The preconditioning procedure of Choi and Merkle has been extended for use in many CFD applications [8–13]. Turkel et al. [14] showed that the conventional compressible algorithms without an adequate modulation of the upwinding or equivalently, the artificial viscosity, do not have the correct asymptotic behavior as the Mach number approaches zero. This problem has drawn considerable attention [15–21]. Guillard and Viozat [17] reported an extension of Roe's FDS upwind scheme that is valid for low Mach number flows. Edwards and Roy [19], and Edwards and Liou [20] reported an extension of the AUSM upwind scheme that is also valid for low Mach number flows.

These works [14–21] also have analyzed the dependence of the variables and the system of equations on the flow Mach number, which implied that the behavior of the system of equations or the convergence characteristics would depend on the flow Mach number. Also, Lee [22,23] developed design criteria for preconditioning methods and analyzed the relationship between convergence characteristics and wave propagation mechanics. However, they did not take notice of the possibility that the convergence characteristics of a specific equation in the system of governing equations might be different from those of the other equations. Lee [24] showed that the convergence characteristics of the energy equation of Euler equations were totally different from those of the continuity and momentum equations. Sesterhenn et al. [25] pointed out that the contribution of the kinetic energy to the total energy at very low Mach numbers gives rise to cancellation errors, which would lead to a deterioration of convergence characteristics of the energy equation. According to our knowledge, no extensive analysis of the convergence characteristics of the preconditioned system of equations has been reported. Thus, the present study was planned to investigate the convergence characteristics of the preconditioned Euler equations in more detail. A perturbation analysis is conducted to analyze the behavior of the governing equations and to search for the relationships between the convergence characteristics and the flow Mach number.

Recently, Sesterhenn et al. [25] analyzed the cancellation mechanisms and reported that cancellation errors played a significant role in calculating low Mach number flows. They also reported that the relative treatments of variables and flux vectors led to improvements in the calculation of very low Mach number flows. However, they did not mention the effects of precision of floating-point variables and the relationship between the relative treatments and convergence rate. Thus, in the present study, the influences of the cancellation errors on convergence characteristics are investigated more thoroughly.

There are some questions about the convergence characteristics of the preconditioned Euler equations. The first question is whether all the equations (continuity, momentum and energy equations) have the same convergence rate in low Mach number flows. If not, then, which is the fastest or slowest? The second question is whether the convergence characteristics of an equation are kept constant regardless of the Mach numbers. If not, then, what is the relationship between the convergence characteristics and the Mach number? The third question is whether there is a Mach number limit preventing an equation from being fully converged. If then, what is the reason for the existence of the Mach number limit?

In Section 2, the preconditioned governing equations are described and the behaviors of the governing equations are analyzed with a perturbation method. Also, the relative treatment of the variables and flux vectors are discussed. In Section 3, the numerical algorithms are described as are the flow conditions and grid systems. Also, the precision of floating-point variables and the numerical methods are discussed and symbolized. In Section 4, the calculation results are presented and discussed.

2. Preconditioned system of equations

2.1. Preconditioned Euler equations

The preconditioned two-dimensional Euler equations are expressed in the following form [7–13,19,20]:

$$\Gamma\frac{\partial Q}{\partial t}+\frac{\partial E}{\partial x}+\frac{\partial F}{\partial y}=0, \tag{2.1.1a}$$

$$Q=\begin{bmatrix} p \\ u \\ v \\ T \end{bmatrix}, \quad E=\begin{bmatrix} \rho u \\ \rho u^2+p \\ \rho uv \\ \rho h_0 u \end{bmatrix} \quad \text{and} \quad F=\begin{bmatrix} \rho v \\ \rho uv \\ \rho v^2+p \\ \rho h_0 v \end{bmatrix}. \tag{2.1.1b}$$

The matrix Γ adopted in the present study is the preconditioning matrix of Choi and Merkle [7] represented in the following form:

$$\Gamma\equiv\begin{bmatrix} \frac{1}{\beta} & 0 & 0 & \rho_T \\ \frac{u}{\beta} & \rho & 0 & \rho_T u \\ \frac{v}{\beta} & 0 & \rho & \rho_T v \\ \frac{h_0}{\beta}-1 & \rho u & \rho v & \rho c_p+\rho_T h_0 \end{bmatrix}, \tag{2.1.2a}$$

$$\beta=M_r^2 c^2, \text{ where } M_r^2=\min(1,M^2). \tag{2.1.2b}$$

The eigenvalues of the preconditioned system of equations in the x-direction are:

$$\lambda_x=u, \quad \frac{1}{2}\left[u(1+M_r^2)\pm\sqrt{u^2(1-M_r^2)^2+4\beta}\right]. \tag{2.1.3}$$

The symbol ρ_T in the preconditioning matrix denotes the derivative of density with respect to temperature. In some of the literature [8–10,12], the derivative of density with respect to temperature is ignored, leading to a slightly different form for the preconditioning matrix

$$\Gamma \equiv \begin{bmatrix} \frac{1}{\beta} & 0 & 0 & 0 \\ \frac{u}{\beta} & \rho & 0 & 0 \\ \frac{v}{\beta} & 0 & \rho & 0 \\ \frac{h_0}{\beta} - 1 & \rho u & \rho v & \rho c_p \end{bmatrix}. \tag{2.1.4}$$

The influence of the derivative of density with respect to temperature will be discussed in detail in Section 2.3.

2.2. Non-dimensionalization

The governing equations (2.1.1) are non-dimensionalized with the thermodynamic and flow quantities at infinite far field: p_∞ (pressure), ρ_∞ (density), T_∞ (temperature), c_∞ (speed of sound), R_∞ (gas constant), γ_∞ (specific heats ratio), and L (characteristic length):

$$\hat{p} = \frac{p}{\gamma_\infty p_\infty}, \quad \hat{\rho} = \frac{\rho}{\rho_\infty}, \quad \hat{T} = \frac{T}{\gamma_\infty T_\infty}, \quad \hat{u} = \frac{u}{c_\infty}, \quad \hat{v} = \frac{v}{c_\infty}, \quad \hat{h}_0 = \frac{h_0}{c_\infty^2}, \tag{2.2.1a}$$

$$\hat{R} = \frac{R}{R_\infty}, \quad \hat{c}_p = \frac{c_p}{R_\infty}, \quad \hat{x} = \frac{x}{L}, \quad \hat{y} = \frac{y}{L}, \quad \hat{t} = \frac{tc_\infty}{L}, \quad \hat{\beta} = \frac{\beta}{c_\infty^2}. \tag{2.2.1b}$$

The speed of sound rather than flow velocity is adopted as the reference velocity for the purpose of representing the non-dimensional flow velocity as a function of Mach number. The "hat" notation stands for non-dimensionalized quantities. Thus, the governing equations become

$$\begin{bmatrix} \frac{1}{\hat{\beta}c_\infty^2} & 0 & 0 & \frac{\hat{\rho}_T \rho_\infty}{\gamma_\infty T_\infty} \\ \frac{\hat{u}}{\hat{\beta}c_\infty} & \hat{\rho}\rho_\infty & 0 & \frac{\hat{\rho}_T \hat{u}\rho_\infty c_\infty}{\gamma_\infty T_\infty} \\ \frac{\hat{v}}{\hat{\beta}c_\infty} & 0 & \hat{\rho}\rho_\infty & \frac{\hat{\rho}_T \hat{v}\rho_\infty c_\infty}{\gamma_\infty T_\infty} \\ \frac{\hat{h}_0}{\hat{\beta}} - 1 & \hat{\rho}\hat{u}\rho_\infty c_\infty & \hat{\rho}\hat{v}\rho_\infty c_\infty & \hat{\rho}\hat{c}_p\rho_\infty R_\infty + \frac{\hat{\rho}_T \hat{h}_0 \rho_\infty c_\infty^2}{\gamma_\infty T_\infty} \end{bmatrix} \frac{c_\infty}{L}\frac{\partial}{\partial \hat{t}} \begin{bmatrix} \hat{p}\gamma_\infty p_\infty \\ \hat{u}c_\infty \\ \hat{v}c_\infty \\ \hat{T}\gamma_\infty T_\infty \end{bmatrix} + \frac{1}{L}\frac{\partial}{\partial \hat{x}} \begin{bmatrix} \hat{\rho}\hat{u}\rho_\infty c_\infty \\ \hat{\rho}\hat{u}^2\rho_\infty c_\infty^2 + \hat{p}\gamma_\infty p_\infty \\ \hat{\rho}\hat{u}\hat{v}\rho_\infty c_\infty^2 \\ \hat{\rho}\hat{h}_0\hat{u}\rho_\infty c_\infty^3 \end{bmatrix}$$
$$+ \frac{1}{L}\frac{\partial}{\partial \hat{y}} \begin{bmatrix} \hat{\rho}\hat{v}\rho_\infty c_\infty \\ \rho\hat{u}\hat{v}\rho_\infty c_\infty^2 \\ \hat{\rho}\hat{v}^2\rho_\infty c_\infty^2 + \hat{p}\gamma_\infty p_\infty \\ \hat{\rho}\hat{h}_0\hat{v}\rho_\infty c_\infty^3 \end{bmatrix} = 0 \tag{2.2.2}$$

and the thermodynamic state equation becomes

$$\hat{p}\gamma_\infty p_\infty = \hat{\rho}\hat{R}\hat{T}\rho_\infty R_\infty \gamma_\infty T_\infty. \tag{2.2.3}$$

Since $\gamma_\infty p_\infty = c_\infty^2 \rho_\infty$ and $\gamma_\infty T_\infty = c_\infty^2 / R_\infty$, the governing equations can be reduced to

$$\begin{bmatrix} 1/\hat{\beta} & 0 & 0 & \hat{\rho}_T \\ \hat{u}/\hat{\beta} & \hat{\rho} & 0 & \hat{u}\hat{\rho}_T \\ \hat{v}/\hat{\beta} & 0 & \hat{\rho} & \hat{v}\hat{\rho}_T \\ \hat{h}_0/\hat{\beta} - 1 & \hat{\rho}\hat{u} & \hat{\rho}\hat{v} & \hat{\rho}\hat{c}_p + \hat{h}_0\hat{\rho}_T \end{bmatrix} \frac{\partial}{\partial \hat{t}} \begin{bmatrix} \hat{p} \\ \hat{u} \\ \hat{v} \\ \hat{T} \end{bmatrix} + \frac{\partial}{\partial \hat{x}} \begin{bmatrix} \hat{\rho}\hat{u} \\ \hat{\rho}\hat{u}^2 + \hat{p} \\ \hat{\rho}\hat{u}\hat{v} \\ \hat{\rho}\hat{h}_0\hat{u} \end{bmatrix} + \frac{\partial}{\partial \hat{y}} \begin{bmatrix} \hat{\rho}\hat{v} \\ \rho\hat{u}\hat{v} \\ \hat{\rho}\hat{v}^2 + \hat{p} \\ \hat{\rho}\hat{h}_0\hat{v} \end{bmatrix} = 0 \tag{2.2.4}$$

and the thermodynamic state equation can be reduced to

$$\hat{p} = \hat{\rho}\hat{R}\hat{T}. \tag{2.2.5}$$

The non-dimensionalized governing equations and the thermodynamic state equation are of the same form as the original equations, respectively. Hereafter, the "hat" notations will be dropped for convenience.

2.3. Behavior of system of equations: perturbation analysis

Some previous works [15–18,21] decomposed the pressure into a thermodynamic pressure and a perturbed pressure expressed as a function of Mach number and showed that the perturbation analysis was a powerful method to explain the behavior of the system of equations. Thus, in the present study, an extended perturbation analysis is conducted to search for the relationship between the convergence characteristics and the flow Mach number. This analysis is confined to low Mach number adiabatic flows in which the variation of the Mach number does not exceed the Mach number itself. Then, due to the definition (2.2.1), the non-dimensionalized flow velocity is $O(M)$, and the variations of the thermodynamic variables are so small that the non-dimensionalized thermodynamic variables are O(1). Thus, the orders of magnitude of the non-dimensionalized quantities are as follows:

$$u, v \sim O(M), \quad p, \rho, T \sim O(1), \quad h_0 \sim O(1), \quad c_p \sim O(1), \quad \beta \sim O(M^2). \tag{2.3.1}$$

Let the perturbation of flow velocity be the order of the Mach number

$$\delta u, \delta v \sim O(M). \tag{2.3.2}$$

Then, the order of the variation in the magnitude of kinetic energy per mass is

$$\delta\left(\frac{u^2+v^2}{2}\right) = u\delta u + v\delta v \sim O(M^2). \tag{2.3.3}$$

In case of an adiabatic condition, the total enthalpy should be invariant

$$\mathrm{d}h_0 = c_p \mathrm{d}T + u\mathrm{d}u + v\mathrm{d}v = 0. \tag{2.3.4}$$

Thus, the order of magnitude of the temperature variation must be $O(M^2)$. The variations of pressure and density can be evaluated with the isentropic relations:

$$\frac{\mathrm{d}p}{p} = \gamma\frac{\mathrm{d}\rho}{\rho} = \frac{\gamma}{\gamma-1}\frac{\mathrm{d}T}{T}. \tag{2.3.5}$$

Since the orders of magnitude of the thermodynamic variables are O(1), the orders of magnitude of the variation of the pressure and density are $O(M^2)$. Thus, the orders of magnitude of the variation of all the thermodynamic variables are $O(M^2)$

$$\delta p, \delta\rho, \delta T \sim O(M^2), \delta h \sim O(M^2). \tag{2.3.6}$$

Now consider the response of the system of equations due to the perturbation (2.3.2). The variation of the convection vector in the x direction can be expressed as follows:

$$\delta E = \begin{bmatrix} \delta(\rho u) \\ \delta(\rho u^2 + p) \\ \delta(\rho u v) \\ \delta(\rho u h_0) \end{bmatrix} = \begin{bmatrix} \rho\delta u + u\delta\rho \\ 2\rho u\delta u + u^2\delta\rho + \delta p \\ \rho u\delta v + \rho v\delta u + uv\delta\rho \\ \rho u(c_p\delta T + u\delta u + v\delta v) + \rho\left(h + \frac{u^2+v^2}{2}\right)\delta u + u\left(h + \frac{u^2+v^2}{2}\right)\delta\rho \end{bmatrix}. \tag{2.3.7}$$

With Eqs. (2.3.2)–(2.3.6), the order of magnitude of the convection vector variation can be expressed in the following form:

$$\delta E \sim \begin{bmatrix} O(M) + O(M^3) \\ O(M^2) + O(M^4) \\ O(M^2) + O(M^4) \\ O(M) + O(M^3) + O(M^5) \end{bmatrix}. \tag{2.3.8}$$

An important aspect of Eq. (2.3.8) is that the magnitude range of the variation terms in the energy equation is wider than that in the other equations. As mentioned by Sesterhenn et al. [25], the contribution of the kinetic energy to the total enthalpy gives rise to cancellation errors, because the difference of the two terms is much smaller than the total enthalpy. Thus, for the same reason, the wider range of the orders of magnitude of the variation of energy flux gives rise to cancellation errors, which implies that the energy equation would suffer more cancellation problems than the other equations.

Now, let the right-hand side vector of the discretized governing equations be considered. It is well known that the methods or schemes for the discretization of the convection flux vectors have great effects on the convergence characteristics of the discretized governing equations [14–20,26]. However, the discretization problem is beyond the concerns of the present study. Thus, a well conditioned or an analytically proven discretization is assumed in the present analysis. Since the effective order of the magnitude of an element is determined by the largest order of magnitude, the effective order of magnitude of the variation of the right-hand side vector in the discretized governing equations can be expressed as follows:

$$\mathrm{RHS} \sim \frac{\Delta t}{\Delta l} \begin{bmatrix} O(M) \\ O(M^2) \\ O(M^2) \\ O(M) \end{bmatrix}. \tag{2.3.9}$$

The notation Δl stands for a spatial grid size such as Δx or Δy. It should be noted that $\Delta l/\Delta t$ has the dimension of velocity and the orders of magnitude of eigenvalues defined in Eq. (2.1.3) are the same as the order of magnitude of the flow velocity. Thus, $\Delta l/\Delta t$ has the order of Mach number if the CFL number is unity. Thus, Eq. (2.3.9) becomes

$$\mathrm{RHS} \sim \begin{bmatrix} O(1) \\ O(M) \\ O(M) \\ O(1) \end{bmatrix}. \tag{2.3.10}$$

From now on, the behavior of the solutions will be investigated. The explicit form of the system of equations is considered for simplicity. In the first place, let the preconditioning matrix ignoring the derivative of density with respect to temperature be considered. From the viewpoint of the order of magnitude, the system of equations can be expressed in the following form:

$$\begin{bmatrix} O(M^{-2}) & 0 & 0 & 0 \\ O(M^{-1}) & O(1) & 0 & 0 \\ O(M^{-1}) & 0 & O(1) & 0 \\ O(M^{-2}) & O(M) & O(M) & O(1) \end{bmatrix} \begin{bmatrix} \Delta p \\ \Delta u \\ \Delta v \\ \Delta T \end{bmatrix} \sim \begin{bmatrix} O(1) \\ O(M) \\ O(M) \\ O(1) \end{bmatrix}. \tag{2.3.11}$$

Therefore, the order of the magnitude of the pressure change is $O(M^2)$ and the order of the magnitude of the velocity change is $O(M)$, which are well matched with Eqs. (2.3.3) and (2.3.7). Meanwhile, the order of the magnitude of the temperature change is O(1), which is not matched with Eq. (2.3.7)

$$\begin{bmatrix} \Delta p \\ \Delta u \\ \Delta v \\ \Delta T \end{bmatrix} \sim \begin{bmatrix} \mathrm{O}(M^2) \\ \mathrm{O}(M) \\ \mathrm{O}(M) \\ \mathrm{O}(1) \end{bmatrix}. \tag{2.3.12}$$

It should be noted that the numerical change of temperature due to the velocity perturbation disregards the Mach number, which may lead to a serious deterioration of the convergence characteristics of the energy equation, especially in very low Mach number flows. It should also be noted that this mismatch between the physical variation of temperature and the numerical change of temperature is due to the characteristics of preconditioning matrix.

Now, let the effects of the derivative of density with respect to temperature in the preconditioning matrix be considered. The derivative of density with respect to temperature derived due to the thermodynamic state equation is as follows:

$$\rho_{\mathrm{T}} = \frac{\partial \rho}{\partial T}\bigg)_p = -\frac{\rho}{T} \sim \mathrm{O}(1). \tag{2.3.13}$$

The term $\Gamma_{4,4}$ of the preconditioning matrix for a thermally perfect gas becomes

$$\rho c_p + h_0 \rho_{\mathrm{T}} = \rho\left(c_p - \frac{h_0}{T}\right) = -\frac{\rho}{T}\frac{u^2+v^2}{2} \sim \mathrm{O}(M^2). \tag{2.3.14}$$

Thus, from the viewpoint of the order of magnitude, the system of equations can be expressed in the following form:

$$\begin{bmatrix} \mathrm{O}(M^{-2}) & 0 & 0 & \mathrm{O}(1) \\ \mathrm{O}(M^{-1}) & \mathrm{O}(1) & 0 & \mathrm{O}(M) \\ \mathrm{O}(M^{-1}) & 0 & \mathrm{O}(1) & \mathrm{O}(M) \\ \mathrm{O}(M^{-2}) & \mathrm{O}(M) & \mathrm{O}(M) & \mathrm{O}(M^2) \end{bmatrix} \begin{bmatrix} \Delta p \\ \Delta u \\ \Delta v \\ \Delta T \end{bmatrix} \sim \begin{bmatrix} \mathrm{O}(1) \\ \mathrm{O}(M) \\ \mathrm{O}(M) \\ \mathrm{O}(1) \end{bmatrix}. \tag{2.3.15}$$

As mentioned in the articles [15,27], with Eq. (2.3.15), the energy equation essentially updates the pressure. The magnitude of the pressure change is $\mathrm{O}(M^2)$. The balance between the update in pressure and temperature is then enforced by the continuity equation. Therefore, the order of magnitude of the temperature change becomes O(1). This is the same result as derived from Eq. (2.3.11). Thus, the derivative of density with respect to temperature does not affect the convergence characteristics.

2.4. Cancellation problems and relative treatments

In low Mach number flows, there is a large difference between a variable and its variation. It is well known that round-off errors occur during numerical calculations if the difference of two numbers is much smaller than either number. Thus, cancellation errors occurring as an accumulation effect of round-off errors would play a significant role in calculating low Mach number flows. Many previous studies [7–10,12–18] used the concept of gauge pressure in which the pressure was decomposed into a constant reference pressure and a gauge pressure, and showed an alleviation of the cancellation problems. Sesterhenn et al. [25] extended this concept and introduced the relative treatments of all the variables and flux vectors as follows:

$$\phi = \bar{\phi} + \phi', \quad \phi = u, v, h_0, p, T, \rho, \tag{2.4.1a}$$

$$E_k = \bar{E}_k + E'_k, \quad E_k = E, F. \tag{2.4.1b}$$

The part with an over-bar stands for a fixed one, while the part with a prime stands for a relative one. Thus, the difference of a variable or a flux vector becomes the difference of a relative variable or a relative flux vector as follows:

$$\mathrm{d}\phi = \mathrm{d}\left(\bar{\phi} + \phi'\right) = \mathrm{d}\phi', \tag{2.4.2a}$$

$$\mathrm{d}E_k = \mathrm{d}\left(\bar{E}_k + E'_k\right) = \mathrm{d}E'_k. \tag{2.4.2b}$$

Thus, governing equations can be represented in the following form:

$$\Gamma \frac{\partial Q'}{\partial t} + \frac{\partial E'_k}{\partial x_k} = 0, \tag{2.4.3a}$$

$$Q' = \begin{bmatrix} p' \\ u' \\ v' \\ T' \end{bmatrix} \quad \text{and} \quad E'_k = \rho u_k \begin{bmatrix} 0 \\ u' \\ v' \\ h'_0 \end{bmatrix} + \left(\rho' u'_k + \bar{\rho} u'_k + \rho' \bar{u}_k\right) \begin{bmatrix} 1 \\ \bar{u} \\ \bar{v} \\ \bar{h}_0 \end{bmatrix} + \begin{bmatrix} 0 \\ p'\delta_{1k} \\ p'\delta_{2k} \\ 0 \end{bmatrix}. \tag{2.4.3b}$$

The effects of the relative treatment on the convergence characteristics will be discussed thoroughly in Section 4.3.

3. Numerical methods

3.1. Discretization

The governing equations (2.1.1) on the (x,y) coordinate system were transformed into the following form on the (ξ,η) generalized coordinate system:

$$\frac{\Gamma}{J}\frac{\partial Q}{\partial t} + \frac{\partial \tilde{E}}{\partial \xi} + \frac{\partial \tilde{F}}{\partial \eta} = 0, \tag{3.1.1a}$$

$$\tilde{E} = \frac{\xi_x E + \xi_y F}{J} = \frac{1}{J}\begin{bmatrix} \rho U \\ \rho U u + \xi_x p \\ \rho U v + \xi_y p \\ \rho h_0 U \end{bmatrix}, \quad \tilde{F} = \frac{\eta_x E + \eta_y F}{J} = \frac{1}{J}\begin{bmatrix} \rho V \\ \rho V u + \eta_x p \\ \rho V v + \eta_y p \\ \rho h_0 V \end{bmatrix}. \tag{3.1.1b}$$

$$J = \frac{\partial(\xi,\eta)}{\partial(x,y)} = \frac{1}{x_\xi y_\eta - x_\eta y_\xi}, \tag{3.1.1c}$$

$$U = \xi_x u + \xi_y v, \quad V = \eta_x u + \eta_y v. \tag{3.1.1d}$$

A finite volume method was used to discretize the preconditioned governing equations. To get the flux vector at the surface of a grid cell, Roe's FDS (flux difference splitting) scheme [17,28] was used. The van Albada limiter [29] was used to avoid numerical oscillations. The LU-SGS (Lower Upper Symmetric Gauss Seidel) scheme [9,11,30] was used for time integration. Convergence rate is greatly dependant on the CFL number, and a larger CFL number gives a faster convergence. In the LU-SGS scheme, it is possible to determine the CFL number for Euler equations as a large one. In the present study, the CFL number was fixed at 1000.

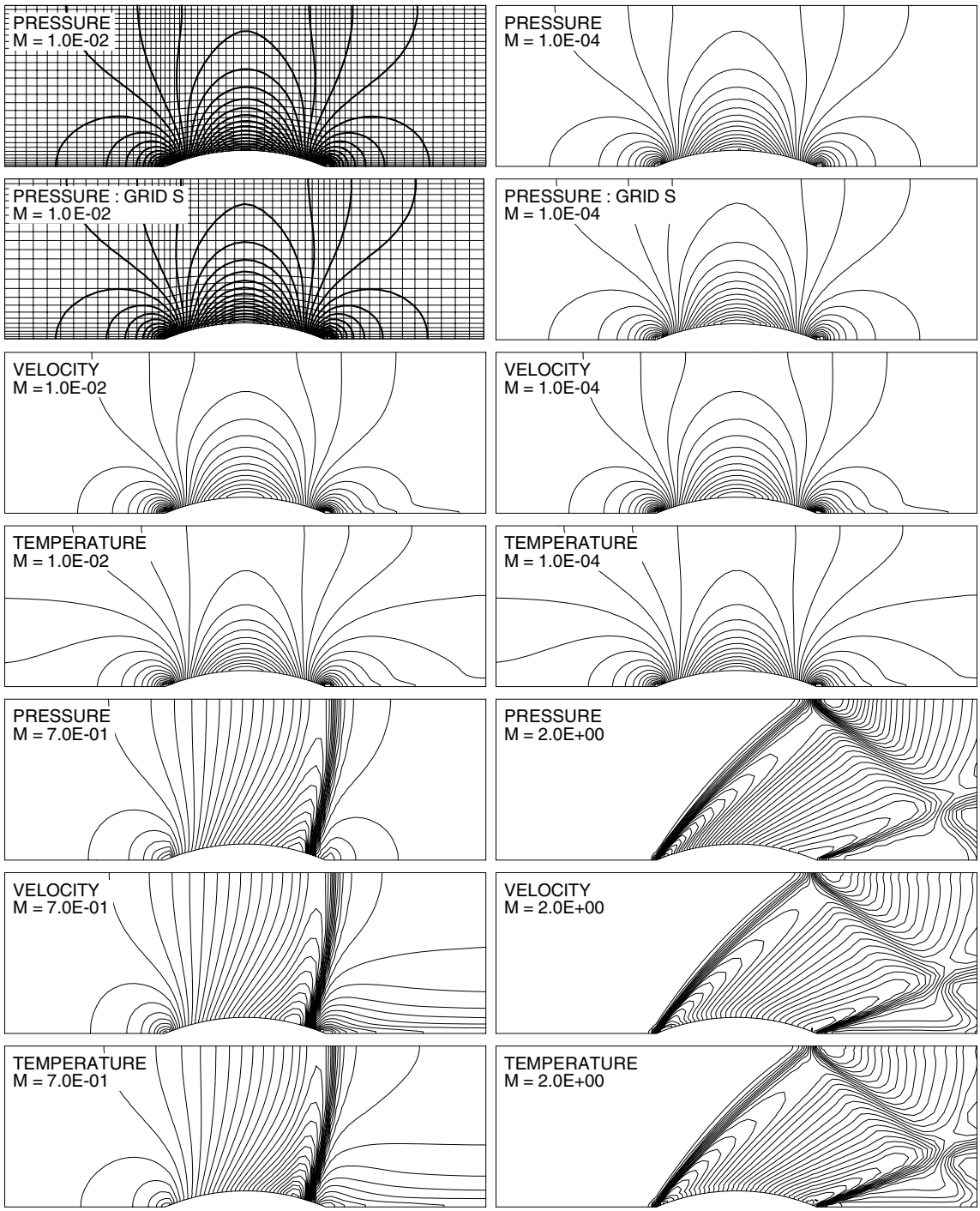

Fig. 1. Contours of pressure, velocity and temperature at various Mach numbers.

3.2. Geometry and grid system

In the present study, inviscid flows through a two-dimensional channel with a 10% circular bump in the middle of the lower wall were calculated. The characteristic length is the height of the channel, L. The length of the circular bump is L and the total length of the channel is $3L$. Calculations were conducted on three kinds of grid systems: grid systems P, S and L. Most of calculations were conducted on grid system P, while the calculations for checking grid independence were conducted on the extra grid systems, grid systems S and L. Thus, if unspecified, grid system P was used. The number of grid points of grid system P, N_G, was 1950(=65[x] × 30[y]). The numbers of grid points of grid systems S and L were 1125(=45[x] × 25[y], 58% of N_G) and 3800(=95[x] × 40[y], 195% of N_G), respectively. Grid points were clustered towards where the gradients of solutions were large and towards upper and lower walls. The figures of grid systems P and S are shown in Fig. 1.

3.3. Flow conditions and boundary conditions

The working fluid is air treated as an ideal gas. The stagnation pressure and temperature is 100 kPa and 300 K, respectively. The initial thermodynamic and flow conditions are calculated based on an assumption of an isentropic process. The inflow and outflow boundaries were specified with the characteristic boundary conditions [26,31,32]. As suggested by Okong'o et al. [32], the density and velocity at the inflow boundary were fixed, and the pressure was updated according to outgoing wave amplitude variations determined from interior points. The pressure at the outflow was fixed, and the remaining wave amplitude variations were determined from the interior points. The pressure, density, temperature and magnitude of velocity on the channel walls were determined to be the same as those on the nearest grid point from the wall, respectively. Also, the direction of the velocity on the slip wall was determined to be tangential to the wall.

3.4. Algorithms and precision of floating point variables

The numerical algorithms used for the present study were realized with the standard C language. The standard C language provides three types of floating point variables: single precision (''float'' in C language), double precision (''double'' in C language) and extended double precision (''long double'' in C language). The ''float'' type variable stores 7 significant digits, the ''double'' type variable stores 15 significant digits, and the ''long double'' type variable stores 18 significant digits. In the present study, two kinds of relative-variable treatments were used: only one for pressure and the other for flux vectors as well as all the variables. In the present study, six combinations of algorithms and precisions were considered. For convenience, some symbols were introduced to distinguish the methods. Most calculations were conducted with method DP. Thus, if unspecified, method DP was used. The meanings of the symbols are described in Table 1.

4. Results

4.1. Verification of computation code

Fig. 1 shows the solutions of the flows at various Mach numbers. In subsonic cases, $M \leqslant 10^{-2}$, the contours of pressure, velocity magnitude and temperature are almost symmetric, respectively. The asymmetric features behind the bump are due to the difference in boundary conditions between the inlet and

Table 1
Symbols for numerical methods

Method	Precision (C language)	Relative variable	Relative vector
SN	Single (float)	–	–
SP	Single (float)	Pressure	–
DP	Double (double)	Pressure	–
DF	Double (double)	All variables	Flux vectors
LP	Extended double (long double)	Pressure	–
LF	Extended double (long double)	All variables	Flux vectors

exit planes. The flow fields at a Mach number of 10^{-4} seem to be almost the same as the flow fields at a Mach number of 10^{-2}. For the purpose of checking grid independence, the pressure fields calculated on the two different grid systems were compared. The pressure fields calculated on grid system S seem to be almost the same as those calculated on grid system P, regardless of the Mach number. This implies that the grid system used in the present study has enough number of grid points. The case with a Mach number of 0.7 showed shock structures over the bump similar to those characteristic of transonic flows over airplane wings. The case with a Mach number of 2.0 showed shock waves in front of the bump, expansion waves, recompression shock waves behind the bump, and reflection shock waves on the upper wall. It may be stated, therefore, that the computation code used in the present study was able to capture the correct features of the flows at all Mach numbers. These results were almost the same as in previously reported studies [12,19].

Also, numerical errors were quantitatively measured in order to verify the accuracy of the computation code. The measured quantities were the changes in the total enthalpy (h_0) and the entropy (s) between the inlet plane and the exit plane of the channel. The change ratios of the total enthalpy and the entropy were defined as follows:

$$\mathrm{CR}(h_0) = \left|1 - \frac{\bar{h}_{0,\mathrm{Exit}}}{\bar{h}_{0,\mathrm{Inlet}}}\right|, \quad \text{where} \quad \bar{h}_0(x) = \frac{\oint \rho u h_0 \,\mathrm{d}y}{\oint \rho u \,\mathrm{d}y}, \tag{4.1.1}$$

$$\mathrm{CR}(s) = \left|1 - \frac{\bar{s}_{\mathrm{Exit}}}{\bar{s}_{\mathrm{Inlet}}}\right|, \quad \text{where} \quad \bar{s}(x) = \frac{\oint \rho u s \,\mathrm{d}y}{\oint \rho u \,\mathrm{d}y}. \tag{4.1.2}$$

The results are shown in Table 2.

The errors of total enthalpy and entropy were very small even at a Mach number of 10^{-2}. Thus, the present computation code did not have a serious defect. The grid independence could be checked according to the errors of the total enthalpy and the entropy on the additional grid systems. Even grid system S showed very small changes of total enthalpy and entropy with respect to grid system P. Also, the changes of total

Table 2
Change ratios of total enthalpy and entropy

Mach number	Grid system	Number of grid points	CR(h_0)	CR(s)
10^{-2}	S	1125(=45[x] × 25[y])	3.67×10^{-9}	3.40×10^{-8}
	P	1950(=65[x] × 30[y])	2.14×10^{-9}	3.17×10^{-8}
	L	3800(=95[x] × 40[y])	1.86×10^{-9}	2.89×10^{-8}
10^{-4}	S	1125(=45[x] × 25[y])	2.52×10^{-13}	6.64×10^{-10}
	P	1950(=65[x] × 30[y])	2.09×10^{-13}	6.60×10^{-10}
	L	3800(=95[x] × 40[y])	1.84×10^{-13}	6.58×10^{-10}

enthalpy and entropy on grid system L were almost the same to those on grid system P. Thus, the grid system used in the present study seems to be a reasonable one.

4.2. Convergence characteristics

The decay of the residuals of pressure, velocity and temperature was calculated in order to quantify convergence characteristics. The absolute value of each residual, rather than the ratio of each residual to its initial value, was evaluated for the purposes of avoiding the dependence on the initial condition and setting

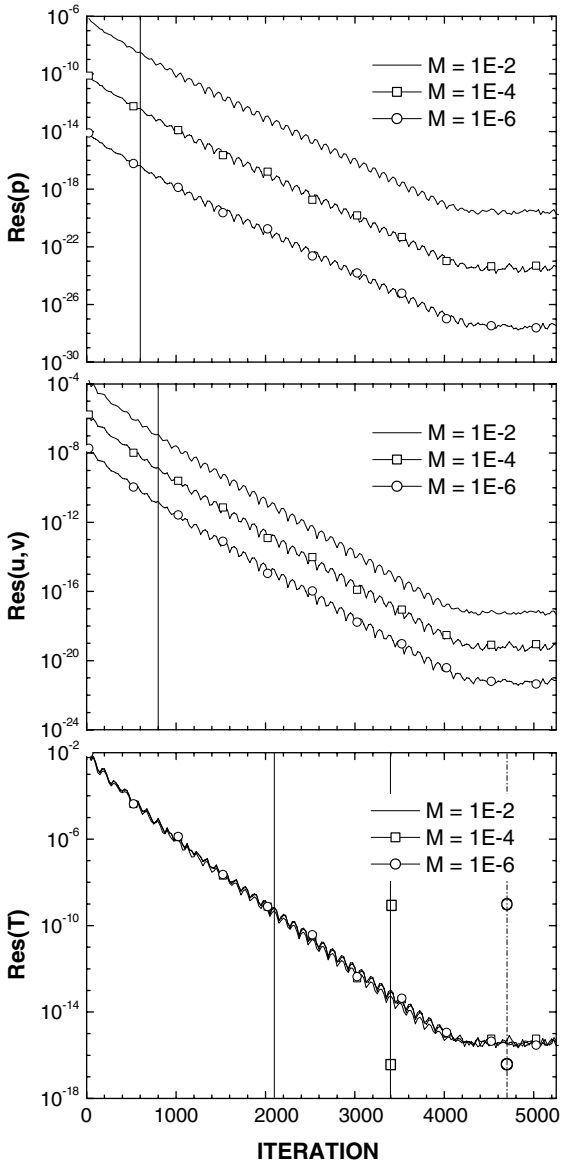

Fig. 2. Convergence histories of pressure, velocity and temperature at various low Mach numbers.

up a unified criterion of convergence. The averaged residuals of pressure, velocity and temperature were defined in the following manner:

$$\mathrm{Res}(p) = \frac{\sum_{i,j}|\Delta p|}{N_{\mathrm{G}}}, \quad \mathrm{Res}(u,v) = \frac{\sum_{i,j}|\Delta u| + |\Delta v|}{N_{\mathrm{G}}}, \quad \mathrm{Res}(T) = \frac{\sum_{i,j}|\Delta T|}{N_{\mathrm{G}}}. \tag{4.2.1}$$

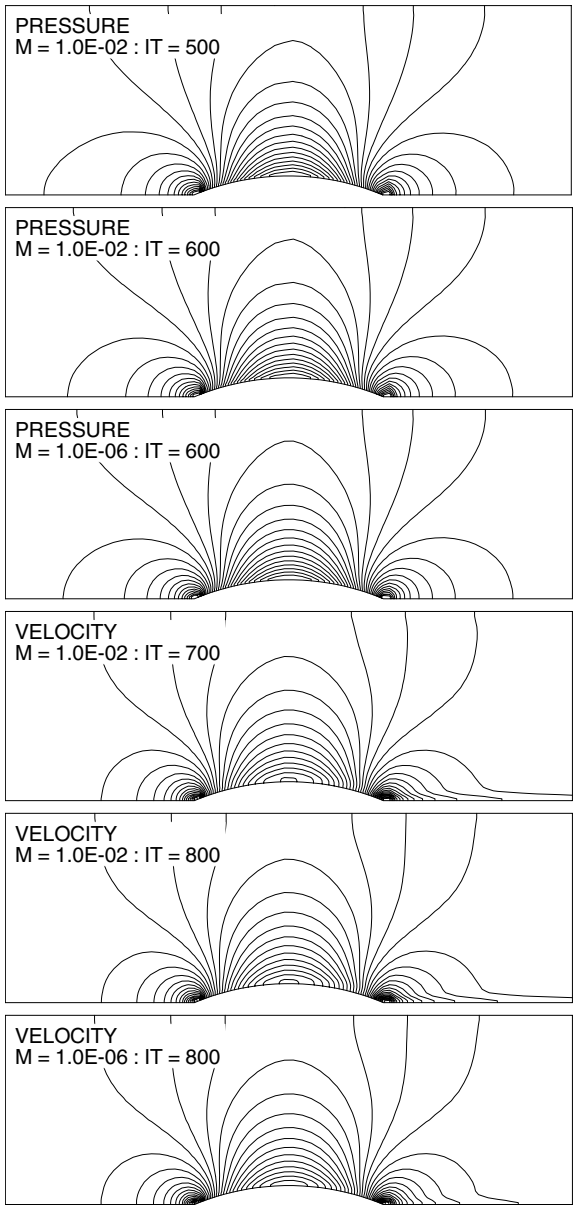

Fig. 3. Changes of pressure and velocity fields due to iteration at various low Mach numbers.

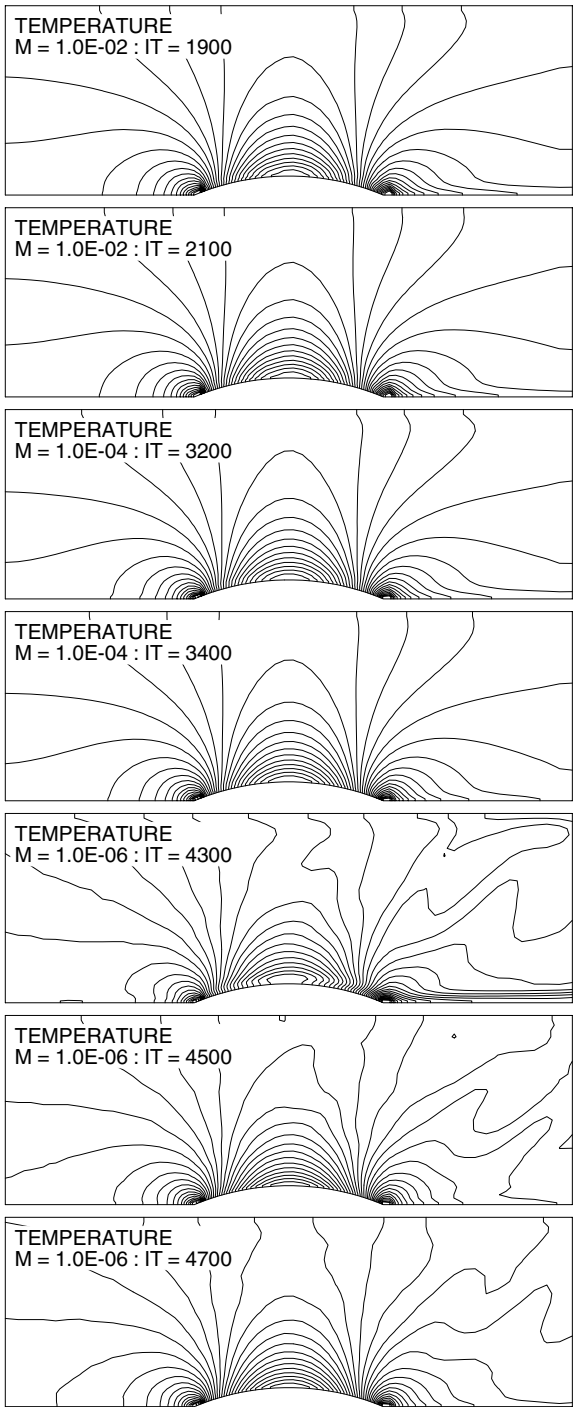

Fig. 4. Changes of temperature field due to iteration at various low Mach numbers.

Fig. 2 shows the decay histories of the residuals of pressure, velocity and temperature versus iteration number. The vertical guidelines indicate the minimum iterations required for sufficient convergence of the governing equations. This will be discussed in the following paragraph. Reducing the Mach number resulted in a smaller residual of pressure and a smaller residual of velocity, while the convergence rates (decay slopes) were almost the same regardless of the Mach number. The gap in the pressure residual between two adjacent curves at a particular iteration number was about 10^{-4} (M_1^2/M_2^2), while the gap in the velocity residual between two adjacent curves at a particular iteration number was about 10^{-2} (M_1/M_2). However, the residuals of temperature coincided regardless of the Mach numbers. These observations were well matched with the perturbation analysis mentioned in Section 2.3.

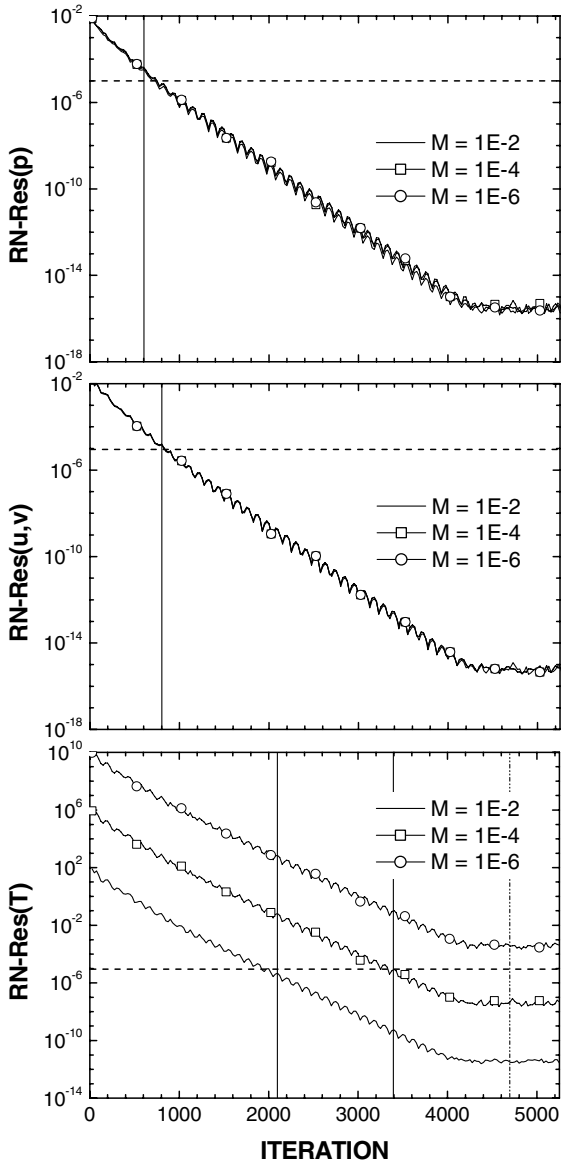

Fig. 5. Convergence histories of pressure, velocity and temperature in renormalized form at various low Mach numbers.

In order to find a criterion for sufficient convergence, the changes in pressure and velocity fields due to iteration were plotted in Fig. 3, while the changes in the temperature fields due to iteration were plotted in Fig. 4. From these figures, it is possible to roughly estimate the minimum number of iterations required for sufficient convergence of an equation. The minimum iteration number required for the converged pressure field was about 600, while the minimum iteration number required for the converged velocity field was about 800. It should be noted that the minimum iterations required for sufficient convergence of pressure or velocity fields were the same, regardless of the Mach numbers. However, the minimum number of iterations required for sufficient convergence of the temperature field depended on the Mach number. Lower Mach-number cases required a higher minimum iteration number for the

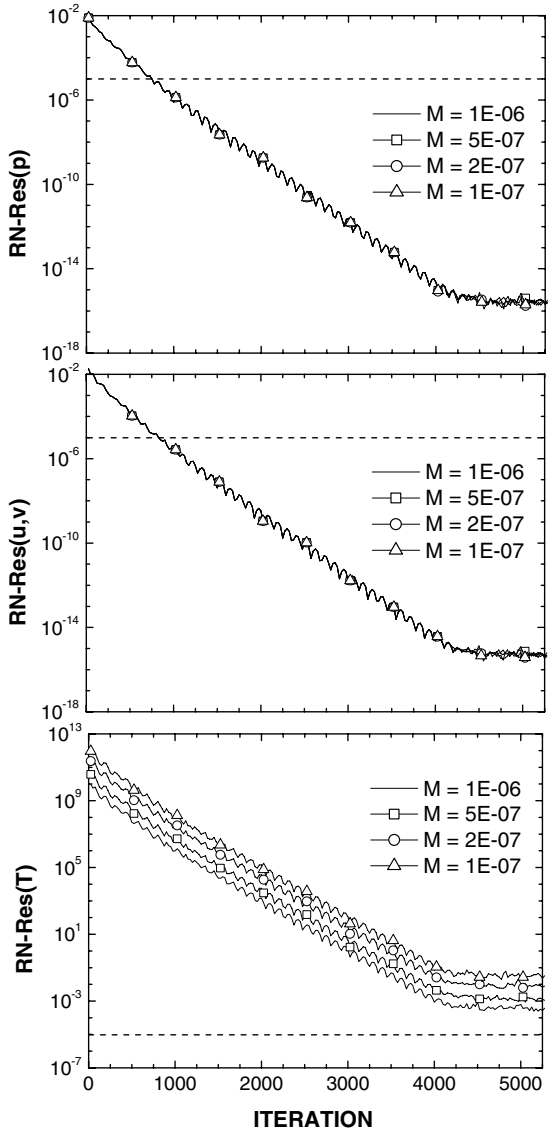

Fig. 6. Convergence histories of pressure, velocity and temperature at very low Mach numbers.

converged temperature field. The minimum iteration number required for the converged temperature field was about 2100 for the case with a Mach number of 10^{-2} and was about 3400 for the case with a Mach number of 10^{-4}. However, it was impossible to obtain a fully converged temperature field when the Mach number was 10^{-6}. There were serious wiggle patterns in the temperature contours, which were due to the cancellation errors. The temperature field with a Mach number of 10^{-6} did not change after about 4700 iterations.

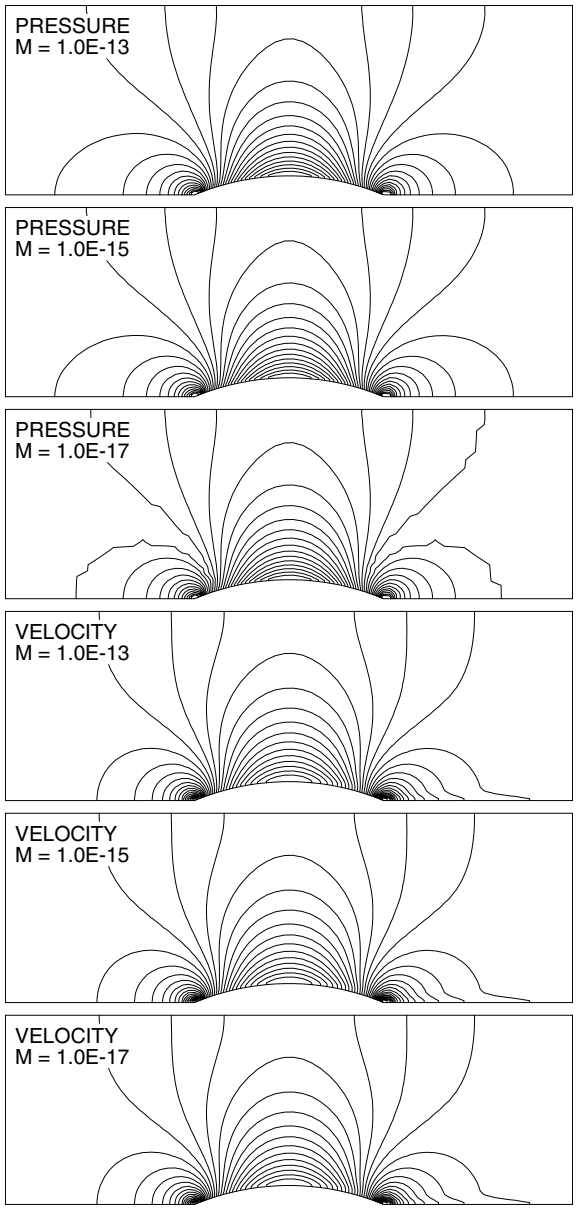

Fig. 7. Pressure and velocity fields at extremely low Mach numbers.

To explain these observations and to set up a unified criterion for sufficient convergence, a renormalization approach was introduced. As mentioned in Section 2.3, for an adiabatic flow condition, the variations of pressure and temperature must be $O(M^2)$ when the variation of velocity is $O(M)$. Therefore, rescaling or renormalizing the residuals in a manner consistent with their own physical behavior would represent the degree of convergence of all the equations with the same criterion. Thus, the residuals of pressure, velocity and temperature were rescaled or renormalized by M_∞^2, M_∞ and M_∞^2, respectively. The renormalized residuals were defined as follows:

$$\text{RN-Res}(p) = \frac{\sum_{i,j}|\Delta p|}{N_G M_\infty^2}, \quad \text{RN-Res}(u,v) = \frac{\sum_{i,j}|\Delta u| + |\Delta v|}{N_G M_\infty}, \quad \text{RN-Res}(T) = \frac{\sum_{i,j}|\Delta T|}{N_G M_\infty^2}. \tag{4.2.2}$$

Fig. 5 compares the decays of the renormalized residuals at Mach numbers of 10^{-2}, 10^{-4} and 10^{-6}. The renormalized residuals of the pressure and the velocity exactly coincided with one another, which was consistent with the observations about the minimum iteration required for enough convergence.

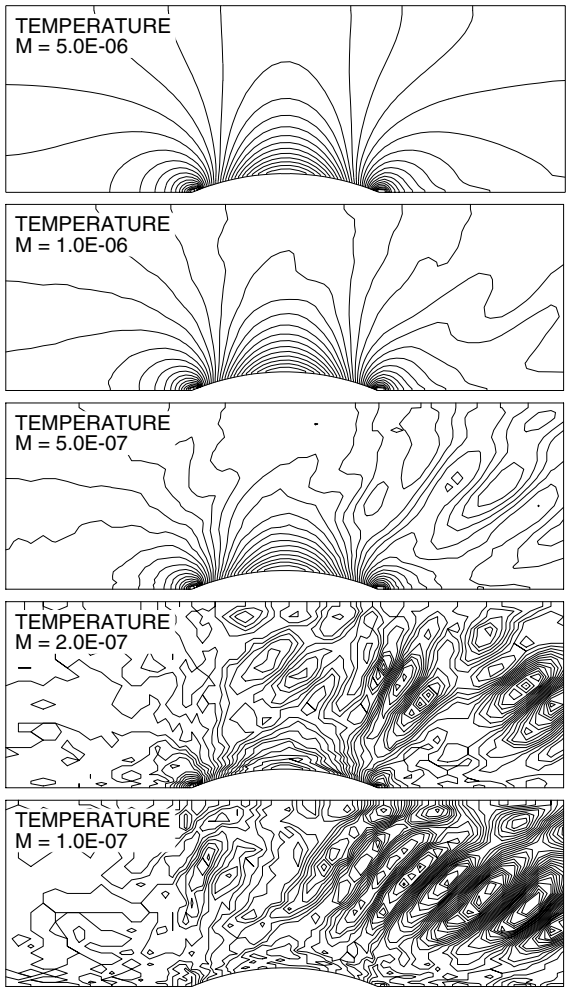

Fig. 8. Temperature fields at very low Mach numbers.

However, the renormalized residuals of temperature did not coincide, but varied with the Mach number. The gap in the renormalized residuals of the temperature between two adjacent curves was about 10^{-4} (M_1^2/M_2^2), which explains the reason why the minimum iteration required for sufficient convergence of temperature fields increased as the Mach number decreased. The vertical guidelines, as mentioned above, indicate the minimum iterations required for sufficient convergence of the governing equations. It should be noted that each horizontal guideline located at 10^{-5} nearly intersects each renormalized residual curve at the point of the minimum iteration required for sufficient convergence of each equation. Thus, the degree of convergence of all equations could be estimated with a unified criterion built on the renormalization (4.2.2).

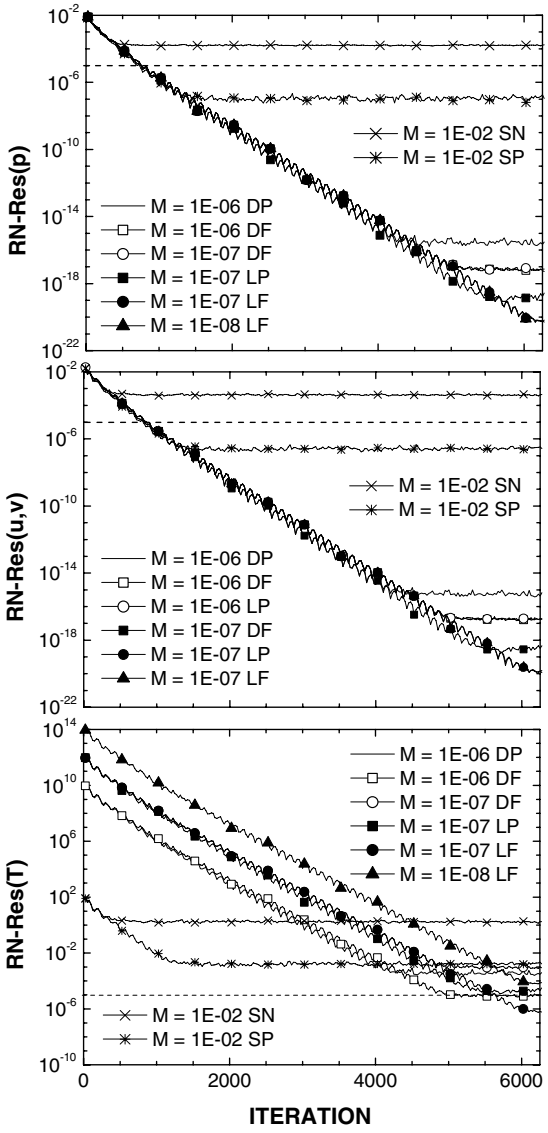

Fig. 9. Comparison of convergence histories of temperature fields among methods SN, SP, DP, DF, LP and LF at various low Mach numbers.

In order to investigate further, the convergence problem at very low Mach numbers, the convergence characteristics of temperature were compared with those of pressure and velocity. Fig. 6 shows the convergence histories of pressure, velocity and temperature at very low Mach numbers below 10^{-5}. All the renormalized residuals of pressure and velocity decayed below the guideline of 10^{-5} within a small number of iterations. However, none of the renormalized temperature residuals dropped below the guideline of 10^{-5}. Fig. 7 shows the contours of pressure and velocity at very low Mach numbers. There were almost no problems in calculating the pressure and velocity fields at extremely low Mach numbers down to 10^{-15} even though such a Mach number hardly has physical meaning. However, there were serious convergence problems in calculating the temperature field. Fig. 8 shows the temperature fields at very low Mach numbers. Numerical oscillations began to appear when the Mach number was 10^{-6} and the situation worsened as the Mach number went below 10^{-6}. The case with a Mach number of 10^{-7} showed few recognizable features in the temperature field.

4.3. Cancellation problems

As mentioned above, the convergence characteristics of temperature worsened as Mach numbers decreased, which made it difficult to calculate the temperature field in a very low Mach number flows. Also, it should be noted that it was impossible to obtain fully smooth temperature contours with method DP when the Mach number is less than 10^{-6}. As mentioned in Section 2.3, this may be due to cancellation errors. In order to clarify the cancellation problem, the effects of the precision of floating-point variables and

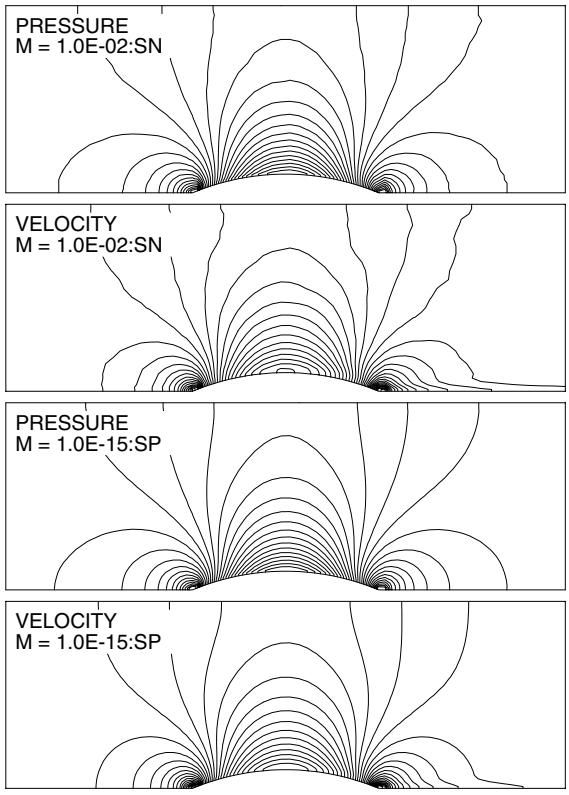

Fig. 10. Comparison of pressure and velocity fields between methods SN and SP at various low Mach numbers.

the effects of the relative treatments were investigated. The calculation results of six kinds of methods (SN, SP, DP, DF, LP and LF) were compared.

Fig. 9 shows the comparison of convergence histories among the methods. It should be noted that all the methods showed almost the same slope of the residual decay until their residuals stopped decaying. This implies that the convergence rate is not affected by the relative treatment or the precision of floating-point variables. Method SN was the first to stop the decay of residuals followed by methods SP, DP, DF, LP and, finally, LF in that order.

Fig. 10 shows the pressure and velocity fields calculated with methods SN and SP. Method SN did not show converged solutions even though the Mach number was 10^{-2}, whereas method SP showed the fully converged pressure and velocity fields even though the Mach number was 10^{-15}. This implies that the relative treatment of pressure guarantees sufficient convergence of the continuity and momentum equations at very low Mach numbers. The temperature fields calculated with these methods are plotted in Fig. 11. Method SN did not show converged solutions even though the Mach number was 10^{-2}, while method SP showed

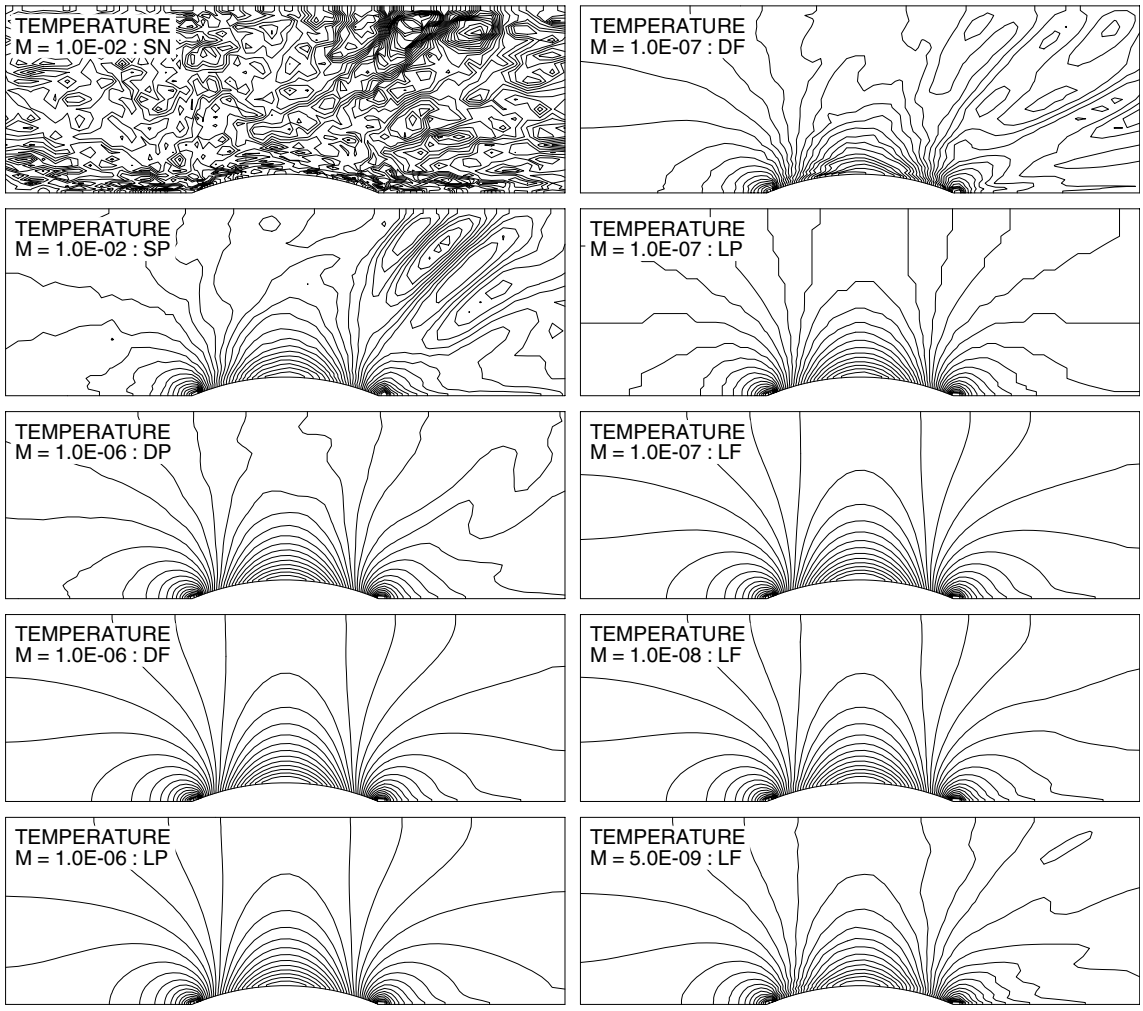

Fig. 11. Comparison of temperature fields among methods SN, SP, DP, DF, LP and LF at various low Mach numbers.

better qualities of temperature contours but did not show a fully converged temperature field even though the Mach number was 10^{-2}. This was due to the fact that method SP had single precision floating-point variables and, thus, suffered serious cancellation problems during the calculation of energy equation. Method DF showed a fully converged temperature field when the Mach number was 10^{-6}, which was impossible with method DP (see Fig. 8). This implies that the relative treatment of flux vectors alleviates the cancellation problems to some extent. Method LP did not show a fully converged temperature field when the Mach number was 10^{-7} but showed better temperature contours than that of method DF. On the other hand, method LF showed a fully converged temperature field until the Mach number went down below 10^{-8}. Some wiggle patterns of temperature contours began to appear when the Mach number was 5×10^{-9}. These facts imply that a higher precision of floating-point variable gives more reduction of cancellation errors and that the precision of floating-point variables is a very important factor especially in the calculations of the temperature field at very low Mach numbers.

5. Conclusions

In the present study, the convergence characteristics of the preconditioned Euler equations were investigated. A perturbation analysis was conducted to investigate the behavior of the governing equations and to search for the relationship between the convergence characteristics and the flow Mach numbers.

An approach for the renormalization of the residuals according to the physical behavior of the variables was introduced in order to estimate the convergence characteristics. The convergence characteristics of the governing equations were well explained with a unified criterion built on the renormalizations.

The convergence characteristics of the continuity and momentum equations were maintained, independent of the Mach number. However, the convergence characteristics of the energy equation changed with the Mach number. A lower Mach number resulted in worse convergence characteristics for the energy equation. These observations were well explained by the perturbation analysis. The perturbation analysis also showed that the convergence characteristics were strongly dependant on the characteristics of the preconditioning matrix.

Some of the convergence problems of the energy equation at very low Mach numbers (below 10^{-6}) were found to be due to cancellation errors. It was shown that the relative treatment of pressure was essential in the calculations of low Mach number flows and that the relative treatment of the variables and flux vectors alleviated the cancellation problems to some extent. It was also shown that using a higher precision of the floating-point variables led to a reduction of cancellation errors and that the precision of floating-point variables was a very important factor in the calculations of the temperature field at very low Mach numbers. However, the convergence rate itself was not affected by the relative treatment or by the precision of floating-point variables.

Acknowledgment

This work was supported by the Research Fund from University of Ulsan. The author acknowledges Professor J. Edwards with whom several conversations benefited the present work.

References

[1] H. Viviand, in: F. Angrand, et al. (Eds.), Numerical Methods for the Euler Equations of Fluid Dynamics, SIAM, Philadelphia, 1985.

[2] R. Peyret, H. Viviand, in: C. Casci (Ed.), Recent Advances in the Aerospace Sciences, Plenum, New York, 1985.
[3] E. Turkel, J. Comput. Phys. 72 (1987) 277.
[4] B. van Leer, W-T. Lee, P. Roe, AIAA paper 91-1552-CP, 1991.
[5] M.A. Storti, C.E. Baumann, S.R. Idelsohn II, WCCM, Stuttgart, 1990.
[6] W.R. Briley, H. McDonald, S.J. Shamroth, AIAA J. 21 (1983) 1467.
[7] Y.H. Choi, C.L. Merkle, J. Comput. Phys. 105 (1993) 207.
[8] J.S. Shuen, K.H. Chen, J. Comput. Phys. 106 (1993) 306.
[9] K.H. Chen, J.S. Shuen, AIAA paper 94-3047, 1994.
[10] K.H. Chen, J.S. Shuen, E. Mularz, AIAA paper 95-0800, 1995.
[11] L.D. Dailey, R.H. Pletcher, AIAA paper 95-1668, 1995.
[12] S. Hsieh, V. Yang, Int. J. CFD 8 (1997) 31.
[13] P. Buelow, D.A. Schwer, J. Feng, C.L. Merkle, AIAA paper 97-2101, 1997.
[14] E. Turkel, A. Fiterma, B. van Leer, in: D.A. Caughey, M.M. Hafez (Eds.), Frontiers of Computational Fluid Dynamics, vol. 215, Wiley, New York, 1994.
[15] R. Klein, J. Comput. Phys. 121 (1995) 213.
[16] H. Bijl, P. Wesseling, J. Comput. Phys. 141 (1998) 153.
[17] H. Guillard, C. Viozat, Comp. Fluid 28 (1999) 63.
[18] H. Guillard, A. Murrone, Comp. Fluid 33 (2004) 655.
[19] J. Edwards, C.J. Roy, AIAA J. 36 (1998) 185.
[20] J. Edwards, M.S. Liou, AIAA J. 36 (1998) 1610.
[21] T. Schneider, N. Botta, K.J. Geratz, R. Klein, J. Comput. Phys. 155 (1999) 248.
[22] D. Lee, J. Comput. Phys. 144 (1998) 423.
[23] D. Lee, J. Comput. Phys. 144 (1998) 460.
[24] S-H. Lee, J. Korean Soc. Aerospace Sci. 29 (7) (2001) 87.
[25] J. Sesterhenn, B. Muller, H. Thomann, J. Comput. Phys. 151 (1999) 597.
[26] E. Turkel, Ann. Rev. Fluid Mech. 31 (1999) 385.
[27] J. Vierendeels, K. Riemslagh, E. Dick, J. Comput. Phys. 154 (1999) 310.
[28] P.L. Roe, J. Comput. Phys. 43 (1981) 352.
[29] P. Arminjon, A. St-Cyr, A. Madrane, Appl. Numer. Math. 40 (2002) 367.
[30] S. Yoon, A. Jameson, AIAA J. 26 (1988) 1025.
[31] D.L. Darmofal, P. Moinier, M.B. Giles, J. Comput. Phys. 160 (2000) 369.
[32] N. Okong'o, J. Bellan, J. Comput. Phys. 176 (2002) 330.